Journal of Materials Chemistry A

ROYAL SOCIETY OF CHEMISTRY

PAPER

View Article Online
View Journal

Cite this: DOI: 10.1039/d6ta01041e

The role of water molecules in piezoelectric-like effects in chitosan-based biodegradable films

Alireza Akbarinejad, *[abc] Holger Fiedler,[d] Donn Adam Gito,[ab] Thomas Loho, [a] Peter C. Sherrell, [ef] Amanda V. Ellis, [e] Kean Aw,[g] Jadranka Travas-Sejdic[bc] and Jenny Malmstrom *[abc]

Soft, flexible piezoelectric polymers have gained increased attention for powering wearable, implantable, and autonomous Internet-of-Things devices. However, the state-of-the-art flexible piezoelectric polymers are fluoropolymers, facing global bans due to environmental concerns. This has led to the development of natural piezoelectric materials. However, achieving reliable piezoelectric performance is challenging due to the limited output of these materials and the complexity of accurately measuring piezoelectric signals, often complicated by other charge-generation mechanisms. Here, flexible and robust chitosan-based films are produced using a simple solvent-casting method. The results show that substrate type and solvent evaporation temperature affect the piezoelectric-like output, with the highest apparent d_{33} of 1.9 ± 0.3 pC N^{-1} observed for chitosan cast on a hydrophilic polystyrene substrate at an evaporation temperature of 40 °C. Importantly, the water content of the films plays a critical role in both mechanical and piezoelectric-like properties. The fully dried films under vacuum exhibit no d_{33} signal, while fully hydrated films show a significantly enhanced response of 11.3 ± 7.0 pC N^{-1}. This work demonstrates the fabrication of biodegradable, piezoelectric-like films and provides key insights into measurement reliability and often-overlooked parameters, such as hydration state, that are crucial for advancing the development of piezoelectric biological materials.

Received 3rd February 2026
Accepted 31st March 2026

DOI: 10.1039/d6ta01041e

rsc.li/materials-a

Introduction

The piezoelectric effect is a unique phenomenon in which specific materials that possess a non-centrosymmetric crystal structure generate an electric charge in response to applied mechanical stress and, conversely, experience mechanical deformation when subjected to an electric field.[1] The ability of piezoelectric materials to efficiently convert between mechanical and electrical energies has led to their widespread use in cutting-edge technologies across multiple industries. As a result, they are widely used in various applications, including sensors,[2,3] actuators,[4,5] piezoelectric motors[6] and energy harvesters.[7–9] Traditional piezoelectric materials, such as natural crystals like quartz and man-made ceramics like lead zirconate titanate (PZT), are the most used materials. In recent years, other inorganic piezoelectrics such as zinc oxide and barium titanate have also attracted significant attention due to their promising piezoelectric properties and lower toxicity.[10,11] However, these materials face several limitations. Crystals and ceramics are typically brittle, making them prone to cracking or mechanical failure under stress. Moreover, they lack flexibility, which restricts their use in applications where mechanical elasticity is required, such as in wearable devices or flexible electronics.[12] Additionally, ceramics like PZT contain toxic elements such as lead, raising significant environmental and health concerns, leading to a demand to develop and adopt more sustainable alternatives.[13,14] Piezoelectric polymers, such as polyvinylidene fluoride (PVDF), offer a solution to the flexibility issue, as they are lightweight and easily processed into thin, flexible films.[15–17] Thus, these polymers are particularly useful in wearable electronics and flexible sensors.[18] However, concerns arise regarding their environmental impact, particularly in terms of degradability, as most synthetic polymers are not biodegradable.[19] In particular, PVDF is facing legislative bans in Europe and globally due to the release of PFAS "forever chemicals", which persist in the environment and pose health risks.[19] The response to these challenges has led to growing

[a]Department of Chemical and Materials Engineering, University of Auckland, Auckland 1142, New Zealand. E-mail: j.malmstrom@auckland.ac.nz; alireza.akbarinejad@auckland.ac.nz

[b]MacDiarmid Institute for Advanced Materials and Nanotechnology, Victoria University of Wellington, P.O. Box 600, Wellington 6140, New Zealand

[c]Centre for Innovative Materials for Health, School of Chemical Sciences, The University of Auckland, 23 Symonds Street, Auckland, New Zealand

[d]National Isotope Centre, New Zealand Institute of Earth Science Ltd, Lower Hutt, New Zealand

[e]School of Chemical and Biomedical Engineering, The University of Melbourne, Parkville, VIC 3010, Australia

[f]School of Science, STEM College, RMIT University, Melbourne, VIC 3001, Australia

[g]Smart Materials and Microtechnologies Group, Department of Mechanical and Mechatronics Engineering, The University of Auckland, Auckland 1010, New Zealand

interest in producing environmentally benign piezoelectric polymers. These materials offer the promise of sustainability and biodegradability, providing an eco-friendly alternative to traditional piezoelectrics.[20,21] However, the development of piezoelectric biological materials comes with its own challenges. One major limitation is their inherently low piezoelectric output, as demonstrated by numerous studies reporting limited piezoelectric signals in these materials.[22–27] For example, cellulose, one of the earliest and most extensively studied piezoelectric biological materials,[24–26] has been reported in the literature to exhibit a d_{33} value of 0.4 pC N^{-1} in its pure form,[22,23] although the authors note that they were unable to locate the original research that measured this value. Collagen, another well-known piezoelectric biological material, has also shown low piezoelectric output, with a d_{33} value of 0.89 pm V^{-1}, reported even in highly oriented collagen such as that found in rat tails.[27] By comparison, a recently developed PZT material prepared *via* a gravity-driven sintering method exhibited a d_{33} value of 595 pC N^{-1}, highlighting the orders-of-magnitude difference between biological and inorganic piezoelectrics.[28] For more detailed information on the piezoelectric outputs of biological materials, recent review papers provide comprehensive insights.[14,20,22] In addition to the low piezoelectricity, another challenge is that other charge-generation mechanisms can complicate the accurate measurement of piezoelectric signals,[29–31] leading to significant discrepancies in reported literature values. Chitosan, a biopolymer that has attracted considerable attention due to its biocompatibility, biodegradability, non-toxicity, and ease of processing, has been reported to exhibit piezoelectric properties.[32] However, as with many other biological materials, there is a wide variation in the reported piezoelectric properties of chitosan. For example, Praveen *et al.* demonstrated non-centrosymmetry in chitosan using XRD analysis and second-harmonic generation experiments.[33] Their investigation of the piezoelectric properties of chitosan films at different temperatures and pressures showed a maximum d_{33} coefficient of 18.6 pC N^{-1} at 300 K. However, the limited experimental details provided make it difficult to assess the reliability of these findings. Marzo *et al.* used a simple solvent casting technique followed by neutralisation in NaOH solution to prepare chitosan films, which were characterised in terms of their piezoelectric properties using piezoresponse force microscopy (PFM).[34] While these results are promising, the use of single-frequency PFM with a soft cantilever (spring constant 0.02–0.8 N m^{-1}) without a comprehensive experimental description on the compensation of electrostatic effects raises concerns about potential non-piezoelectric contributions, influencing the measured values.[35,36] While direct comparison between these reports is difficult due to differences in film properties, other studies have reported no piezoelectric output for chitosan films. For instance, Prokhorov *et al.* investigated a chitosan-$BaTiO_3$ composite film for tissue engineering and, although they reported a d_{33} output of 11.24 pC N^{-1} for the composite using ferroelectric hysteresis curves, they noted that their measurements did not detect a piezoelectric response from pure chitosan.[37]

The observed discrepancies in piezoelectric properties of biological materials across the literature, including chitosan, is partly due to differences in experimental techniques, film processing methods and interpretations of data. Another key challenge in comparing the piezoelectric performance of bio-based polymers like chitosan arises from their ability to adopt different structural conformations such as different molecular conformation, inter-chain interactions, and supramolecular arrangements that can be highly sensitive to processing conditions.[38] For instance, a recent study by Jacopo Nicoletti *et al.* demonstrated that incorporating chitin nanocrystals into natural chitosan-based thin films could achieve d_{33} values of up to 18.7 ± 1.1 pm V^{-1}, among the highest reported for chitosan- and chitin-based materials.[39] Since chitin is the precursor of chitosan and its chemical structure is very similar, and no additional dipole alignment treatment was applied, the observed enhancement further highlights how the piezoelectric properties of biological materials strongly depend on processing conditions that define their structural and conformational states. A particularly underexplored yet critical factor is the hydration state of the biological material films. Chitosan, in particular, has a high capacity to absorb. moisture,[40] which can influence its mechanical properties[41] and crystallinity.[42] Water molecules within the polymer matrix can modify hydrogen bonding networks, affect dipole reorientation, and potentially affect piezoelectric properties of biological materials. While previous reports have noted the influence of humidity on piezoelectricity, to the best of our knowledge no systematic studies have examined how hydration alters material properties in ways that lead to changes in piezoelectric performance. Table S1 summarises a few published studies that mention the effect of humidity on piezoelectric output. As shown, in all cases the underlying mechanisms remain unaddressed, representing a significant knowledge gap in the field. Therefore, the core novelty of this work lies in elucidating how the hydration state influences material properties and how this relates to the observed piezoelectric behaviour. This insight is particularly important given the large number of studies reporting piezoelectric behaviour in biological materials without adequately considering the role of humidity.

Challenges in accurately measuring the piezoelectricity of biological materials highlight the relatively immature state of the field, in which accurate characterisation protocols and material consistency are still being established. Therefore, despite the growing literature on piezoelectric biological materials, reliably characterised examples remain rare. This highlights an urgent need to develop reliable piezoelectric biological materials and establish accurate characterisation methods.

In this work, we deliberately use the term "piezoelectric-like" rather than "piezoelectric" properties. The measured d_{33} signals in biological material films are strongly affected by external factors such as humidity, which can modify mechanical properties, influence ionic mobility, or trigger phase transitions (*e.g.*, glass transition). These effects can contribute to d_{33} meter readings through both piezoelectric and non-piezoelectric mechanisms. Because it is difficult to fully separate genuine piezoelectric behavior from other charge-generation

phenomena, we adopt this cautious terminology to describe the electromechanical responses observed in our study.

Here, we prepare chitosan films using a simple solvent-casting method and characterise their piezoelectric output using a d_{33} meter. We explored parameters that affect the piezoelectric-like properties of chitosan films, including substrate type, evaporation temperature and water content. The optimised film that was prepared on a hydrophilic polystyrene film at 40 °C exhibited a measured apparent d_{33} piezoelectric coefficient of 1.9 ± 0.3 pC N^{-1}. Notably, water content was found to be critical for generating a measurable piezoelectric response: humidified chitosan films produced a significantly enhanced d_{33} of 11.3 ± 7.0 pC N^{-1}, whereas vacuum-dried films showed no detectable output. Nanoindentation and X-ray diffraction (XRD) analyses indicate that a combination of crystalline transitions and variations in the reduced modulus across different hydration states may contribute to the observed changes in d_{33}. Our findings establish a reliable approach for characterising piezoelectricity in chitosan, and also reveal, for the first time, how hydration state, selection of substrate and casting temperature critically influence its piezoelectric-like response. These insights are essential for advancing this field and the development of applications of piezoelectric biological materials.

Results and discussion

Fabrication and characterisation of chitosan films

Chitosan films were prepared using a simple solvent-casting method. This involved dissolving chitosan in a 1% (v/v) acetic acid aqueous solution at a concentration of 1.5% (w/v), casting the solution onto a tissue culture polystyrene Petri dish substrate (area 28.3 cm^2), and evaporating the solvent in an oven to form a solid film (Fig. 1A). This method produced a uniform and flexible film that could be easily removed from the surface, resulting in a freestanding film (Fig. 1B). The film's thickness could be controlled by adjusting the volume of chitosan solution applied to the substrate. As shown in Fig. 1C, casting 0.18, 0.35 and 0.70 mL of chitosan solution per cm^2 of substrate produced films with thicknesses of 22.0 ± 0.7 μm, 48.4 ± 6.2 μm, and 77.6 ± 1.8 μm, respectively. The film prepared from 0.35 mL per cm^2 of chitosan solution was consistently easy to peel from the substrate and offered an optimal balance between mechanical robustness and flexibility. Therefore, this film was selected for subsequent experiments. The FTIR spectrum of the chitosan film is shown in Fig. 1D. Since chitosan is derived from the partial deacetylation of chitin, a process that converts *N*-acetylglucosamine units into glucosamine, the FTIR spectrum of chitosan typically exhibits characteristic peaks associated with both chitin and chitosan.[43] The peaks at 2872 and 2928 cm^{-1} correspond to the anti-symmetric and symmetric stretching vibrations of CH_2, respectively. The band at 1635 cm^{-1} has been widely attributed to the C=O double bond (amide I) stretching vibration in the literature.[44,45] However, this region can also be influenced by the H–O–H bending vibrations of absorbed water molecules, which exhibits a peak near this wavenumber.[46] Given that the chitosan used in this study is more than 75% deacetylated, most nitrogen atoms are expected to occur as amines, with some remaining as amides. Therefore, the peak at 1540 cm^{-1} is likely due to N–H bending, overlapping with the N–H (amide II) stretching vibration.[47,48] The strong peaks in the 950–1190 cm^{-1} range arise from C–N stretching vibrations and overlap with vibrations from the carbohydrate ring.[47] N–H and O–H stretching occurs in the broad region between 3000 and 3700 cm^{-1},[44,47] a region that may also be influenced by the O–H stretching vibrations from water content present in the films.[49]

The tensile test data for the 48.4 μm chitosan film at 0.1% s^{-1} (based on the original length) exhibits a characteristic two-stage linear behavior before failure (Fig. 1E). In the initial region, up to a tensile strain of about 2%, the chitosan film behaves elastically, indicating that the material is deforming in a linear, reversible manner. The Young's modulus of the chitosan film was calculated using the slope of the stress–strain curve in the elastic region between 0–0.5% tensile strain and was found to be 2.3 ± 0.3 GPa, which is consistent with the values reported for chitosan films in the literature.[50] This strain range was chosen for the calculation of Young's modulus because the transition from linear to non-linear behavior occurs gradually, and 0–0.5% represents the most consistent and clearly linear region across all samples (Fig. S1). After this elastic regime, the material reaches its yield point, marking the onset of plastic deformation. At this stage, the curve displays a small decrease in stress due to a localised reduction in the cross-sectional area of the chitosan film, a phenomenon called necking.[51] Beyond the yield point, at a strain of about 3–5%, the material enters a second linear region, suggesting further elongation with a smaller increase in stress. In this second phase, the material continues to plastically deform but continues to bear increasing loads until it eventually breaks. Additional stress–strain curves from repeated tensile tests are provided in the SI (Fig. S1). As seen, these data demonstrate high repeatability in the elastic region used for calculating Young's modulus, confirming the reliability of the measurements. Additionally, the chitosan film demonstrates excellent flexibility, as illustrated in Fig. 1B. These findings suggest that the chitosan film possesses moderate elastic stiffness and experiences notable plastic deformation before failure, making it suitable for applications that require a balance of strength and flexibility. To further assess mechanical properties, a cyclic compression test was performed by applying a 1 N force to the chitosan film for 200 cycles, while monitoring displacement. A comparison of the first and last 20 cycles (Fig. S2) shows no significant change in the displacement amplitude or waveform, indicating minimal mechanical degradation during cyclic loading. This result further confirms the mechanical robustness and fatigue stability of the films. The surface roughness of the chitosan films were impacted by the presence of small particles that remained undissolved in the chitosan solution, even after prolonged stirring. These particles led to a rough surface texture, as verified by atomic force microscopy (AFM) imaging (Fig. 1F). After vacuum filtration to remove the insoluble particles, the films prepared from the filtered solution were noticeably more transparent than their unfiltered counterparts

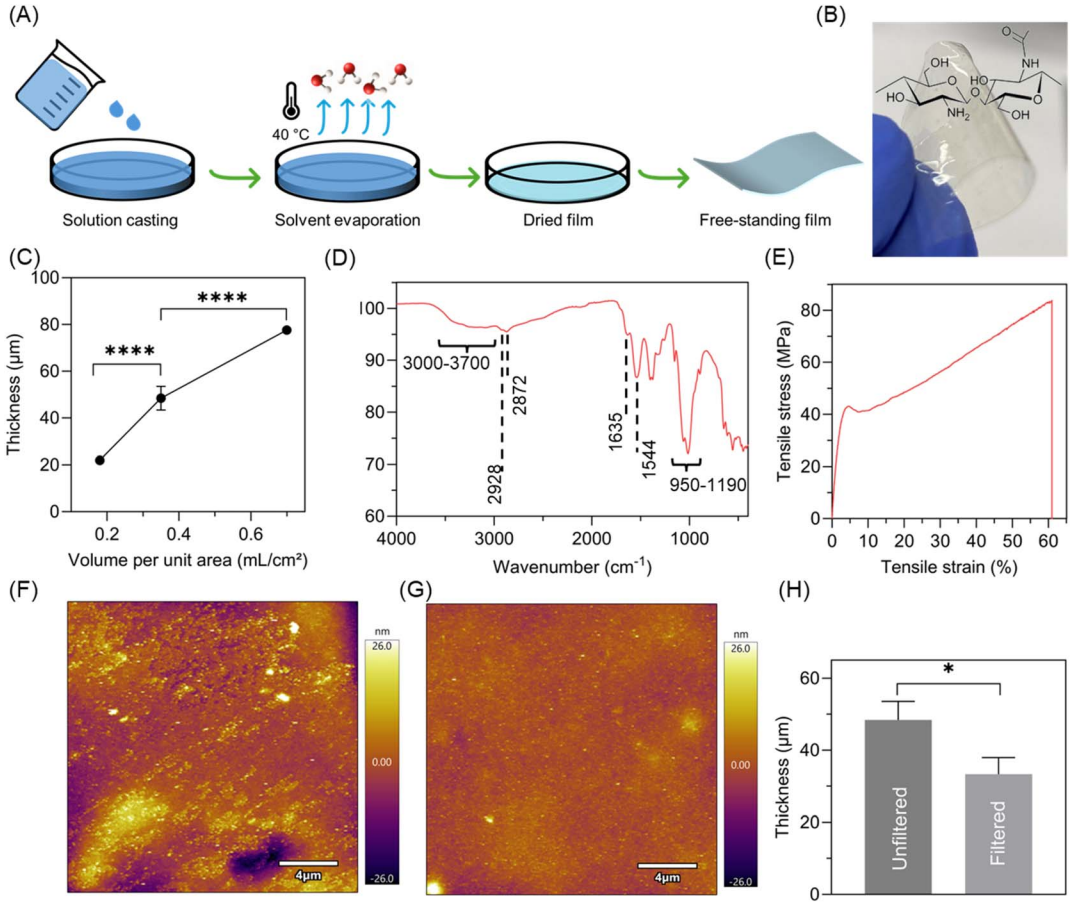

Fig. 1 (A) The steps taken for the preparation of chitosan films. (B) Photograph of the free-standing, flexible chitosan film prepared using the solvent casting method. (C) Plot of chitosan film thickness as a function of the volume of chitosan solution applied per cm^2 of substrate area. Error bars represent standard deviation based on 3–4 samples, with three measurements per sample ($n = 9$–12). Statistical significance: ****$p < 0.0001$ (based on one-way ANOVA ($\alpha = 0.05$), and Tukey's HSD multi comparison tests). (D) FTIR spectrum of chitosan film with the characteristic chitosan peaks indicated. (E) Tensile stress–strain curve of a rectangular chitosan film (1.0 cm wide × 2.0 cm long) tested at a strain rate of 0.1% s^{-1} (F and G) AFM tapping mode height images of chitosan films cast from (F) unfiltered and (G) filtered chitosan solutions and (H) their corresponding thickness measured with a high accuracy digimatic indicator. Error bars represent standard deviation based on 3 samples, with three measurements per sample ($n = 9$). Statistical significance: *$p < 0.1$ (based on unpaired t-test).

(Fig. S3), with AFM confirming the improved smoothness (Fig. 1G). Filtration also affected the film thickness, as the filtered solution produced a thinner film (33.3 ± 4.6 μm) compared to the non-filtered solution (48.4 ± 6.2 μm), likely due to the removal of particulate material during the filtration process (Fig. 1H). The surface morphology of the chitosan films was further examined using SEM. As shown in Fig. S4A and B, both the unfiltered and filtered chitosan films exhibit a compact, featureless structure. Similar structural characteristics for chitosan films have been reported in the literature.[52]

Piezoelectricity of chitosan films

The piezoelectric output of the chitosan film was measured using a d_{33} meter (Fig. S5). The film exhibited a measurable apparent d_{33} signal, which reversed in sign upon inversion of the sample, confirming the piezoelectric origin of the response (Fig. S6). Reported d_{33} values were obtained by averaging the absolute values of the forward and reverse measurements. The chitosan film prepared from unfiltered chitosan solution showed an average apparent d_{33} value of 1.9 ± 0.3 pC N^{-1}. The film prepared from filtered solution exhibited a similar value of 2.0 ± 0.6 pC N^{-1}. For the remainder of the study, the film prepared from the unfiltered solution was used, as the filtration step added unnecessary processing complexity without producing a significant improvement in piezoelectric performance. The measured d_{33} values from chitosan films are particularly promising when compared to the near-zero d_{33} signals observed in our lab for various other biological materials (Fig. 2A). The measured d_{33} values in our lab for some biological materials are significantly lower than the reported piezoelectric outputs in the literature.[53–60] There are several potential reasons for these discrepancies. Some reported d_{33} values for biological materials in the literature are based on piezoresponse force microscopy (PFM) measurements. The improper use of PFM, such as utilising soft cantilevers, can lead to incorrect and exaggerated d_{33} signals.[61] Some other studies have characterised piezoelectric output using methods that

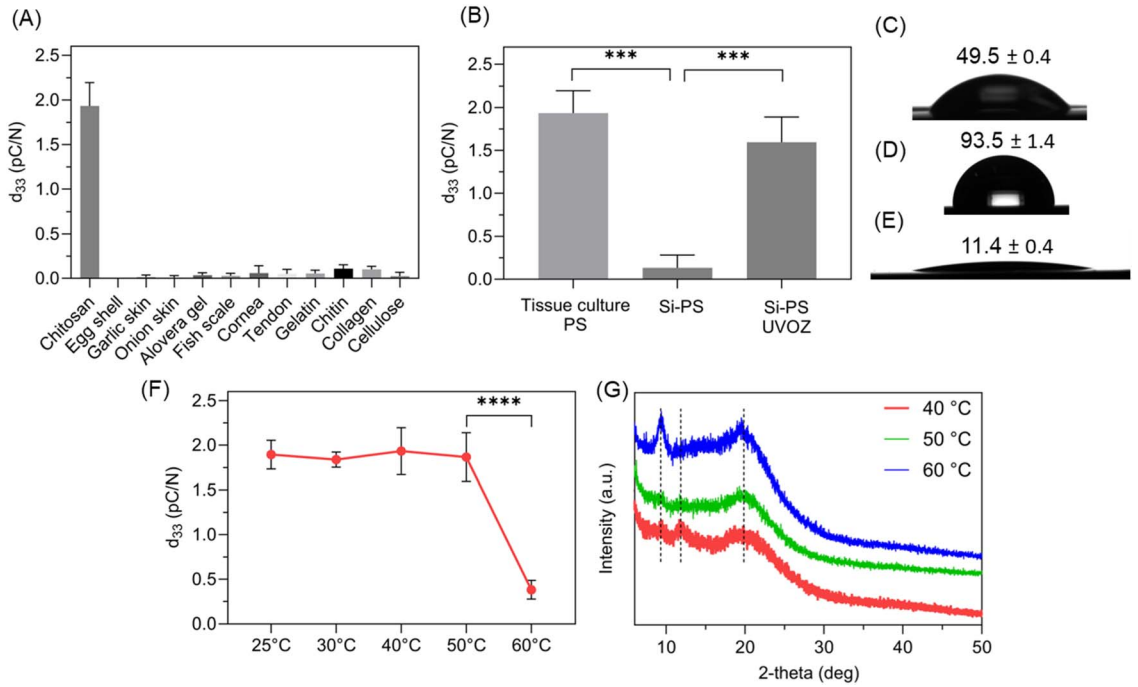

Fig. 2 (A) d_{33} piezoelectric measurements of our chitosan film and various biological materials reported in the literature as exhibiting piezoelectric properties. (B) d_{33} piezoelectric measurements of chitosan films prepared on tissue culture polystyrene dishes and spin-coated polystyrene substrates with and without UV/ozone treatment. Water contact angle results for: (C) polystyrene from tissue culture-modified dishes, (D) polystyrene spin-coated onto silicon wafer and (E) polystyrene spin-coated onto silicon wafer after 30 minutes of UV/ozone treatment. (F) d_{33} signal measurement of chitosan films prepared on tissue culture polystyrene at different evaporation temperatures. (G) XRD patterns of chitosan films prepared at different drying temperatures. All the chitosan films in this figure were prepared using 0.35 mL cm^{-2} of unfiltered chitosan solution. Error bars represent standard deviation based on 2–3 samples, with three measurements per sample ($n = 6$–9). Statistical significance: ****$p < 0.0001$, ***$p < 0.001$ (based on one-way ANOVA ($\alpha = 0.05$)).

involve contact-separation, which, as we demonstrated in our earlier work, can result in significant charge generation from contact electrification (triboelectricity), a phenomenon distinct from piezoelectricity.[30]

We explored several parameters that might affect the piezoelectric performance of chitosan films. One of the parameters is the choice of substrate for solvent casting. To evaluate this influence, we prepared chitosan films on a number of polystyrene substrates, including tissue culture Petri dishes and spin-coated polystyrene films on silicon wafers (Fig. S7). As shown in Fig. 2B, the chitosan film prepared on the spin-coated polystyrene did not exhibit a significant piezoelectric output in contrast to the value of 1.9 ± 0.3 pC N^{-1} obtained with the tissue culture Petri dish. However, after treating the spin-coated polystyrene with UV/ozone for 30 minutes, the chitosan film prepared on this substrate showed an apparent d_{33} values of 1.6 ± 0.3 pC N^{-1} (Fig. 2B). Fig. 2(C–E) illustrate water contact angle measurements on various polystyrene surfaces, including the tissue culture polystyrene Petri dish, spin-coated polystyrene, and UV/ozone-treated spin-coated polystyrene. As anticipated, both the tissue culture polystyrene Petri dish and UV/ozone-treated polystyrene surfaces exhibited hydrophilic properties, with water contact angle values of 49.5 ± 0.4 and 11.4 ± 0.4, respectively, likely due to the presence of polar oxygen-containing groups. In contrast, the spin-coated polystyrene displayed hydrophobic characteristics, evidenced by a water contact angle of 93.5 ± 1.4. These results support the hypothesis that interactions between chitosan and oxygen-containing groups on hydrophilic polystyrene surfaces promote structural alignment within the chitosan film, thereby enhancing the d_{33} output. The difference in d_{33} values observed between tissue culture polystyrene and UV/ozone-treated polystyrene may be attributed to the varying degrees of oxidation (and thus hydrophilicity) of the two substrates. As shown in Fig. S8, chitosan films prepared on several other substrates, including silicon wafers, gold-coated silicon wafers, and glass, did not produce a significant d_{33} output, further highlighting the importance of substrate type on the piezoelectric behavior of the resulting film. Additionally, we found that the evaporation temperature during solvent casting also affected the d_{33} output (Fig. 2F). Notably, the d_{33} from chitosan films was comparable at different casting temperatures between 25 °C and 50 °C, with a significant decrease observed at 60 °C casting temperature. Fig. 2G presents the XRD spectra of chitosan films prepared at different drying temperatures. The film dried at 40 °C shows a semicrystalline structure with characteristic peaks at approximately $2\theta = 9°$, 12°, and 20°, consistent with the previous studies.[39] Notably, the intensity of the peak at 12° decreases significantly when the drying temperature is increased to 50 °C and disappears completely at 60 °C. This peak is assigned to the hydrated crystalline form of chitosan, and its disappearance at higher drying temperatures indicates a crystalline transition

from the hydrated to the dehydrated form. This observation is consistent with the findings of Philip-Kunio Naito *et al.*, who reported a facile crystalline transition of chitosan from hydrated to anhydrous form above 60 °C in the presence of acetic acid.[62] Accordingly, the significant decrease in the measured d_{33} signal at 60 °C can be attributed to this crystaline structural transition from hydrated to dehydrated chitosan.

Water content has been shown to significantly influence the piezoelectric performance of biological materials.[63,64] In this study, we investigated how varying water content affects both the mechanical and d_{33} response of chitosan films. To prepare films with different water contents, chitosan films were first cast by evaporating the solvent in an oven at 40 °C, called ambient chitosan. These films were then either placed in a vacuum oven at 40 °C for 24 hours to remove residual water molecules, called dried, or exposed to saturated water vapor to fully hydrate the films, called hydrated. As shown in Fig. 3A, vacuum drying resulted in a weight loss of 35.7 ± 4.4 mg, while hydration led to a weight gain of 129.8 ± 15.1 mg in the chitosan films. Assuming the vacuum-dried sample contains 0% water, the ambient and humidified films are estimated to have approximately 19% and 52% water content, respectively. Fig. 3B shows the apparent d_{33} signal outputs for these films. The vacuum-dried chitosan film exhibited a negligible piezoelectric-like response, whereas the hydrated film demonstrated a significantly enhanced signal with an apparent d_{33} value of 11.3 ± 7.0 pC N^{-1}. These results highlight water content as a critical parameter in modulating the piezoelectric-like behavior of chitosan. To gain further insight into this behavior, we evaluated the mechanical properties of the films using nanoindentation. In our previous work, we demonstrated that the bulk mechanical properties of biological materials can differ significantly from their surface properties.[65] Since the d_{33} measurements originate from the bulk of the material, it is essential to assess the bulk mechanical properties to establish a meaningful correlation between the d_{33} response and mechanical properties. To achieve this, we employed the "continuous measurement of X" (CMX) nanoindentation technique, which enables the evaluation of dynamic mechanical properties as a function of indentation depth. As shown in Fig. 3C, the storage modulus of the ambient chitosan film decreased with increasing indentation depth and plateaued at approximately 1 μm (corresponding to a load of ~3500 μN), a phenomenon broadly observed for soft materials.[66] A similar trend was observed for the vacuum-dried film, although the modulus stabilised at a higher load of ~5000 μN (Fig. S9A). Although the hydrated film exhibited some variability in the CMX data due to its very low hardness values, its modulus also decreased with depth and eventually stabilised beyond 1.2 μm, corresponding to ~30 μN load (Fig. S9B). To ensure mechanical properties were measured from depths representative of bulk behavior, we conducted further nanoindentation measurements at controlled loads: 5000 μN for the ambient and vacuum-dried films, and 80 μN for the hydrated film using accelerated property mapping (XPM) method. The ambient film exhibited a reduced modulus of 3.9 ± 0.2 GPa, which increased to 6.1 ± 0.2 GPa in the vacuum-dried sample. In contrast, the water-saturated film displayed a significantly lower reduced modulus of 17.0 ± 8.0 MPa, consistent with its softer nature (Fig. 3D). These observations align with existing literature that reports an inverse relationship between humidity level and the modulus of chitosan.[41]

The observed trend in d_{33} response can be understood using the following relationship from linear piezoelectric theory:[67]

$$d_{33} = \frac{e_{33}}{C_{33}^{E}} \quad (1)$$

where d_{33} and e_{33} are the piezoelectric coefficients at constant stress and constant strain, respectively. C_{33} is the elastic constant along the same axis, which we measured by nanoindentation. Thus, in pressure ranges consistent with Hook's law, softer materials (lower C) have higher d_{33} values. Thus, our experimental findings, showing highest d_{33} for the hydrated (soft) film and lowest for the vacuum-dried (stiff) film, are in excellent agreement with theoretical predictions. While the variation in d_{33} correlates well with the differences in reduced modulus across samples with varying water content, the underlying mechanisms are likely more complex. In addition to changes in elasticity, other factors such as alterations in the hydrogen bonding network within the chitosan matrix may also contribute to the observed piezoelectric-like behavior as the water content changes.[26] Fig. 3E compares the FTIR spectra of chitosan films at different hydration states. As shown, the hydrated sample exhibits a significant increase in the intensity of the broad peak at 3000–3700 cm^{-1} and the peak at 1635 cm^{-1}, while these peaks are significantly reduced in the dried sample. These changes can be attributed to the varying presence of water molecules in the films, higher in the hydrated and lower in the dried samples, and to alterations in the N–H, O–H and C═O stretching vibrations caused by hydrogen bonding between water molecules and the N–H, O–H and C═O groups of chitosan.[42,49] These interactions may play a significant role in the variations observed in the d_{33} response of chitosan films under different hydration conditions. To explore whether the piezoelectric-like response could be reversibly modulated through hydration and drying, we conducted a simple rehydration test. Vacuum-dried chitosan films were stored under ambient laboratory conditions (RH of ~50–60%, 20–22 °C) for about 1 month, allowing them to gradually reabsorb moisture. The apparent d_{33} signal of these rehydrated films increased to 1.4 ± 0.2 pC N^{-1}, which is comparable to the films stored continuously at ambient conditions (Fig. 3F). This indicates the potential for storing chitosan films in a dry state and rehydrating them prior to use, enabling consistent and predictable piezoelectric performance in real-world settings.

Additionally, in soft hydrated biological material films, contributions from ions need to be considered. In the present system, chitosan films are prepared by dissolving chitosan in dilute acetic acid, which results in protonated amine groups ($-NH_3^+$) along the polymer backbone and associated acetate counterions (CH_3COO^-) within the film. In systems containing mobile ionic species, other charge-generation mechanisms have been reported that can produce signals resembling a piezoelectric response. These include piezoionic effects,

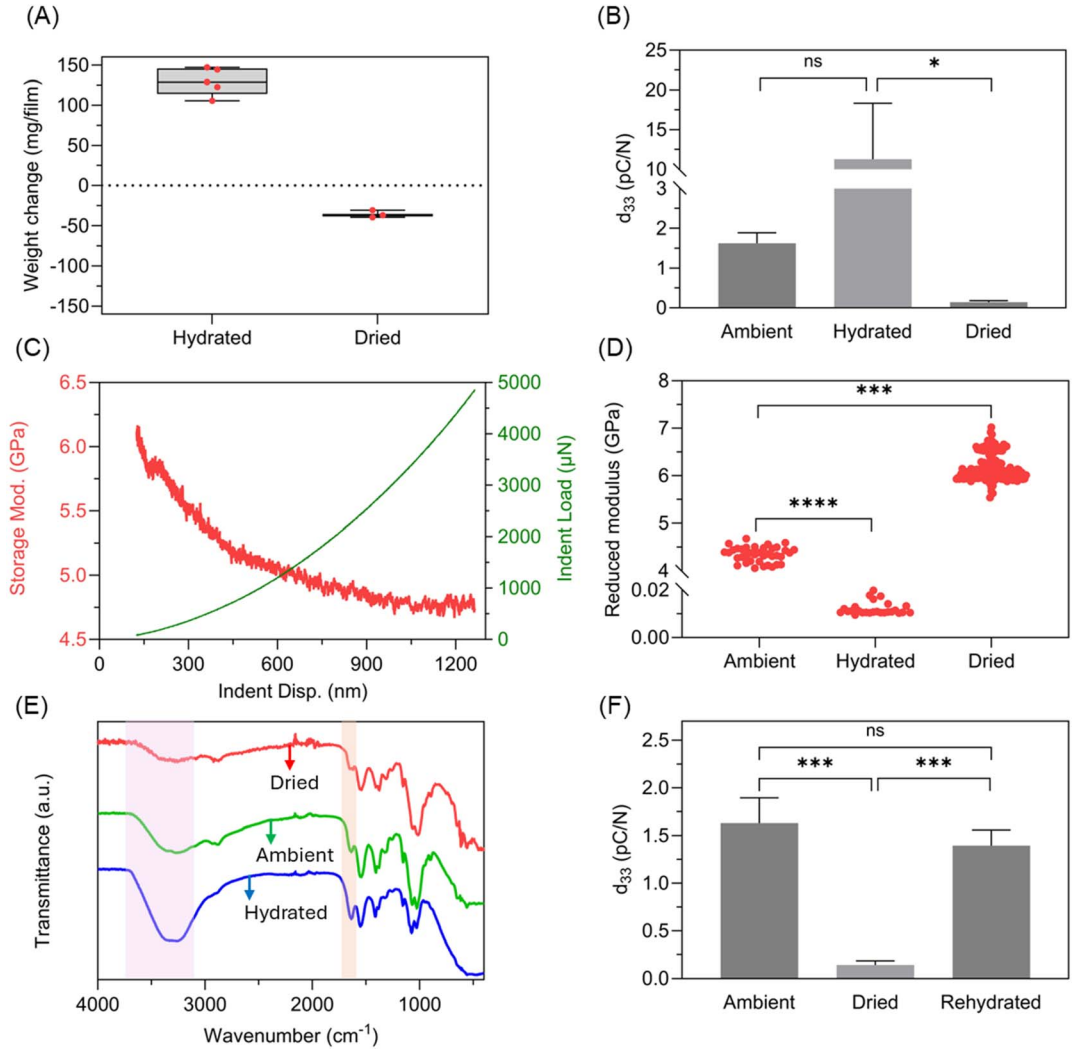

Fig. 3 (A) Change in mass (mg) of circular chitosan films (area = 28.3 cm^2) following treatment by either hydration or vacuum drying. The data reflect the net weight change associated with water absorption or loss under the respective conditions. (B) d_{33} piezoelectric measurements of chitosan films at different humidification states. Error bars represent standard deviation based on 3 samples, with three measurements per sample ($n = 9$). Statistical significance: *$p < 0.1$ (based on one-way ANOVA ($\alpha = 0.05$), and Tukey's HSD multi comparison tests). (C) Storage modulus and indentation load as a function of indentation depth for chitosan film prepared by oven drying at 40 °C (ambient chitosan), measured using the CMX nanoindentation technique. (D) Average reduced modulus of chitosan films prepared at 40 °C (ambient), fully hydrated and vacuum-dried, measured using the XPM nanoindentation method. Data were obtained from two independent samples per condition, with a minimum of 18 measurements per sample ($n = 36$–148). Statistical significance: ****$p < 0.0001$, ***$p < 0.001$ (based on one-way ANOVA ($\alpha = 0.05$), and Tukey's HSD multi comparison tests). (E) FTIR spectra of chitosan films at different hydration states, highlighting hydration-dependent changes in the O–H/N–H (purple) and C═O (orange) stretching regions associated with hydrogen bonding. (F) Comparison of the apparent d_{33} piezoelectric response of chitosan films under three conditions: stored continuously under ambient conditions (~50–60% RH, ~20–22 °C), vacuum-dried, and vacuum-dried followed by rehydration under ambient laboratory conditions for one month. Error bars represent standard deviation based on 3 samples, with three measurements per sample ($n = 9$). Statistical significance: ***$p < 0.001$ (based on one-way ANOVA ($\alpha = 0.05$), and Tukey's HSD multi comparison tests).

where mechanical deformation leads to redistribution of ions and the generation of an electrical potential.[68,69] In addition, electromechanical responses associated with pressure-induced liquid-to-crystalline phase transitions have also been reported in some ionic liquid systems.[70,71] While such mechanisms may contribute to measured electromechanical signals in highly hydrated soft materials with high ionic concentrations, their influence in the present system is expected to be limited due to the relatively low concentration of ionic species and the fact that any remaining ions are largely associated with the polymer chains rather than present as freely mobile species. Nevertheless, the possible contribution of ionic effects cannot be completely excluded, which is one of the reasons the measured response is conservatively described as piezoelectric-like.

An overview of the factors influencing the piezoelectric-like performance of chitosan films is provided in Table 1, which highlights the relative importance of key processing parameters on the measured d_{33} output. A broader consideration of our

Table 1 Summary of the influence of key processing parameters on the measured d_{33} output of chitosan films, identified from the experimental results obtained in this study

Parameter	Effect on d_{33}	Importance	Rationale
Hydration state	Fully dried: ~0.0 pC N^{-1} Fully hydrated: ~11.3 pC N^{-1}	Very important	Water significantly enhances reduced modulus and hydrogen bonding
Substrate type	Hydrophilic polystyrene yields highest d_{33} (~1.9 pC N^{-1})	Very important	Substrate potentially affects drying dynamics and chain alignment
Solvent evaporation temperature	Stable d_{33} readings (~1.8–1.9 pC N^{-1}) when films were cast at temperatures between 25–50 °C, with a significant reduction in d_{33} values outside this range	Important	Influences, crystaline structure, hydrogen bonding and chain alignment
Solution filtration	Filtered: ~1.9 pC N^{-1} Nonfiltered: ~2.0 pC N^{-1}	Not important	Filtered insoluble material likely has similar properties to soluble chitosan
Ionic mobility effects	Possible minor contribution	Negligible	Low ionic concentration; NH_3^+/CH_3COO^- largely bound to polymer chains rather than freely mobile

findings highlights both the potential and the challenges of developing chitosan-based piezoelectric materials. As summarised in Table 1, factors such as hydration state, substrate type, and solvent evaporation temperature have a pronounced effect on the measured d_{33} values, highlighting the sensitivity of chitosan films to processing and environmental conditions. In particular, hydration plays a critical role: while fully hydrated films can yield d_{33} values above 11 pC N^{-1}, fully dried films show almost no measurable response. This sensitivity raises important concerns about long-term signal stability under ambient conditions. Our measurements, however, indicate that chitosan films stored under typical laboratory conditions (relative humidity ~50–60%, temperature 20–22 °C) remain relatively stable, with d_{33} values decreasing only slightly from 1.9 to 1.6 pC N^{-1} over a 96-days period (Fig. S10). Additionally, the d_{33} response of the ambient chitosan films was measured at multiple time points over 48 hours by fixing the film between the d_{33} electrodes and without moving it, ensuring all measurements were taken at the same location. Each measurement applied a dynamic force of 250 mN at 110 Hz for ~10 s, corresponding to ~1100 loading cycles per measurement. As shown in Fig. S11, the d_{33} values remain largely stable over time, indicating that the films maintain their electromechanical response under repeated dynamic loading and exhibit good mechanical stability under these measurement conditions. Although the effect of humidity on piezoelectric output has been observed in previous studies, our work represents the first systematic investigation linking humidity to changes in the material properties of chitosan films and, in turn, to the observed variations in d_{33} output (Table S1). Taken together, these results emphasise that while the piezoelectric response of chitosan films is significantly lower compared to inorganic materials, careful control of processing parameters and environmental conditions can yield reproducible and stable performance. Future work should address the fundamental mechanisms underlying hydration effects and develop optimised device architectures to enable practical applications in sensing, energy harvesting, and bioelectronics.

Conclusions

In conclusion, we successfully prepared flexible and mechanically robust chitosan films using a simple solvent-casting method and thoroughly characterised their structural, morphological, and mechanical properties through FTIR, XRD, SEM, AFM, tensile tests and nanoindentation. Our investigation into the piezoelectric-like properties of the films revealed that the substrate type and evaporation temperature significantly influence their d_{33} output. The optimised film, cast on hydrophilic polystyrene at 40 °C, exhibited a reliable apparent d_{33} piezoelectric coefficient of 1.9 ± 0.3 pC N^{-1}. Furthermore, we demonstrated that water content plays a critical role in modulating the d_{33} response. Hydrated chitosan films showed a markedly enhanced apparent d_{33} value of 11.3 ± 7.0 pC N^{-1}, whereas vacuum-dried films exhibited a complete loss of d_{33} response. Nanoindentation measurements revealed substantial changes in the reduced modulus with hydration state, decreasing in hydrated films and increasing in vacuum-dried ones (ambient sample ~3.9 GPa, dried sample ~6.1 GPa, hydrated sample ~0.02 GPa), suggesting that mechanical stiffness may be a contributing factor to the observed variations in d_{33} output. In contrast to chitosan, a wide range of other biological materials previously reported as piezoelectric showed no measurable d_{33} output in our tests. The findings from our work highlight the need for reliable, reproducible results and for careful design considerations when working with piezoelectric-like biological materials. Our results position chitosan as a promising material with moderate piezoelectric output for use in future biodegradable electronic applications. Importantly, the strong dependence of the electromechanical response on hydration highlights both a key design consideration for practical device development and potential opportunities for

applications operating in naturally moist environments, such as biomedical interfaces.

Experimental

Materials

Chitosan (≥75% deacetylated, 50 000–190 000 Da), glycine, gelatine (from porcine skin) were procured from Sigma-Aldrich. Acetic acid AR glacial 99.7% was purchased from ECP Labchem (New Zealand). Poled polyvinylidene fluoride (PVDF) film (thickness of 50 μm) was purchased from PolyK (USA). Sylgard 184 polydimethylsiloxane (PDMS) elastomer base and curing agents were obtained from Dow Corning (Elizabethtown, KY, USA). Type 1 (Milli-Q) water (resistivity: 18.2 MΩ cm, Milli-Q Direct, MilliPore) was used throughout the work.

Fabrication of chitosan films

First, a 1% (v/v) solution of acetic acid in Milli-Q water was prepared. Chitosan was then mixed with the acetic acid solution at a concentration of 1.5% (w/v) and stirred for 24 hours to ensure complete dissolution. To produce chitosan films of varying thicknesses, 0.18, 0.35 and 0.70 mL of chitosan solution per cm^2 of substrate were added to the lower portion of Petri dishes made of tissue culture polystyrene (Falcon ref. 353002, 60 mm diameter). For films formed on silicon wafers or gold-coated silicon wafers, a PDMS mold with an inner diameter of 60 mm was prepared and attached to the substrate surface, creating a designated area for the chitosan solution casting. The substrates were then placed in an oven at different temperatures (25, 30, 40, 50, and 60 °C) to evaporate the solvent. Films prepared at 25–30 °C were dried over 7 days, while those prepared at 40–60 °C were dried over 3 days. Once the solvent had completely evaporated, a solid chitosan film formed, which was then carefully removed from the substrate to obtain a free-standing film. For filtered chitosan films, the preparation followed the same process, with the only difference being that before casting onto the substrate, the chitosan solution was vacuum filtered using Whatman® quantitative filter papers, Grade 40.

PDMS mold preparation

A circular PDMS mold with an inner diameter of 60 mm was prepared for solution casting on silicon wafers and gold-coated silicon wafer substrates. To fabricate this, a PDMS prepolymer was prepared by mixing the PDMS base and curing agent in a 10 : 1 ratio, followed by stirring for 10 minutes. The mixture was then placed under vacuum for approximately 1 hour to remove any trapped air. After degassing, the prepolymer solution was poured into a mold made from two Petri dishes with diameters of 60 mm and 94 mm. The prepolymer was cured in an oven at 65 °C for 1 hour, after which the cured PDMS was carefully removed from the mold.

d_{33} measurements

The apparent d_{33} outputs were measured in both forward and reverse orientations using a quasi-static d_{33} piezometer (Sinocera, YE2730A) under a dynamic force of 0.25 N at a frequency of 110 Hz, with the films placed between two round-shaped probe electrodes. The d_{33} device used in this work lacked a sensor for static force measurement. Hence, to ensure consistency and repeatability, for all the measurements electrodes were tightened until the film was securely held in place and did not move between the electrodes. To ensure accurate measurements, the d_{33} meter was calibrated prior to the measurements according to the procedure below:

(1) The instrument was first calibrated using the PZT standard supplied by the manufacturer using the ×1 range.

(2) An electrically poled PVDF, with a d_{33} value of 20–25 pC N^{-1} (according to the manufacturer) was measured in the ×1 range to confirm the instrument accurately detected the signal from a soft polymer.

(3) The instrument was then switched to the ×0.1 range and roughly calibrated using PVDF.

(4) Finally, fine-tuning was performed to ensure the instrument read zero for several non-piezoelectric polymers (such as Teflon and non-piezoelectric nylon PA6).

Due to the absence of a static force sensor in our Sinocera d_{33} measurement system, we conducted independent validation measurements using a PKD3 d_{33} meter equipped with a static force sensor. Using the same electrode tightening procedure, the applied static force was determined to be approximately 0.35 N. Fig. S12 compares the d_{33} values obtained from the two instruments for our ambient piezoelectric chitosan film and electrically poled PVDF film. The strong agreement between the two datasets confirms the reliability of the d_{33} measurements reported in this study.

Attenuated total reflection-fourier transform infrared (ATR-FTIR) spectroscopy

ATR-FTIR spectra were obtained using a PerkinElmer AUTR Two FTIR spectrometer. Each measurement consisted of 4 scans at a resolution of 4 cm^{-1}, with the spectra recorded over the range of 4000 to 450 cm^{-1}.

Atomic force microscopy (AFM)

AFM in tapping mode was employed to visualise the surface morphology of chitosan films made from both unfiltered and filtered chitosan solutions. The chitosan films were adhered to a steel puck using double-sided tape, and imaging was conducted with a Cypher ES Instrument (Oxford Instruments, United States) utilizing Tap150AL-G probes (Budget Sensors, Bulgaria).

X-ray diffraction (XRD)

XRD patterns were collected with a PANalytical Empyrean powder X-ray diffractometer operating at 45 kV and 40 mA. A standard Cu X-ray source with a Kα1 wavelength of 1.5418 Å was employed. Materials were scanned over a two-theta range of 5–50° at a rate of ≈1.25° per min.

Sputter gold coating and scanning electron microscopy (SEM)

A 5 nm layer of gold was sputter-coated onto the chitosan films using a Q150R sputter coater (Quorum Technologies, UK) at a current of 30 mA and a deposition rate of 3 nm min^{-1}. SEM imaging was performed using a Zeiss Crossbeam 350 FIB-SEM instrument operating at an accelerating voltage of 5 kV.

Mechanical properties

Tensile testing. Prior to tensile testing, the films were cut into strips measuring 1.0 cm in width and 2.0 cm in length using scissors, and their thickness was measured with a high accuracy digimatic indicator (Mitutoyo ID-H0530E). Tensile tests were conducted at room temperature (21 °C) using an Instron 3360 machine (Instron Corporation, MA, USA). The films were mounted between the upper and lower clamps of the tensile tester, and the tensile test was conducted at a strain rate of 0.1% s^{-1}.

Nanoindentation testing. Nanoindentation characterisation of the chitosan films was carried out using a Hysitron TI950 Triboindenter (Bruker, Minnesota) equipped with a Performech II control module and a nanoDMA III transducer, enabling it to perform continuous measurement of X (CMX) and accelerated property mapping (XPM) capabilities. A three-sided pyramidal diamond Berkovich indenter tip was used for all measurements. The chitosan films, supported on polystyrene Petri dish substrates, were mounted onto a mild steel base using a thermoplastic cyanoacrylate adhesive without detaching them from the Petri dish substrate. A magnetic base of the instrument minimised lateral movement during testing. To evaluate nanomechanical properties at varying depths, the constant strain rate CMX procedure was used with a ramp-up applied load, a dynamic frequency of 220 Hz, and a variable dynamic load to maintain the constant strain rate. Once the appropriate indentation depth and corresponding load were identified using CMX, the XPM procedure was used to determine the reduced modulus values of the sample. XPM measurements were conducted under load-controlled mode of 5000 μN for both ambient and vacuum-dried films, and 80 μN for humidified films, with a spacing of 50 μm between each indentation point in a 5 × 5 grid at three different areas on the surface of each sample. The Oliver–Pharr method was applied to the unloading segments of the load–displacement curves to calculate the reduced modulus using Hysitron TriboScan software.[72] The calculated reduced modulus (E_r) represents a combination of the elastic moduli of the indenter (E_i) and the sample (E_s) affected by the Poisson's ratio of the indenter (ν_i) and the sample (ν_s), expressed by the following relationship:

$$\frac{1}{E_r} = \frac{1-\nu_i^2}{E_i} + \frac{1-\nu_s^2}{E_s} \quad (2)$$

Given the significant difference between the modulus of the diamond indenter ($E_{diamond}$ = 1140 GPa) and that of the chitosan films (<10 GPa), the very small value of the Poisson's ratio of the indenter ($\nu_{diamond}$ = 0.07), and assuming similar Poisson's ratio values across samples (ν_s = 0.5 for most polymers),[73] the reduced modulus values calculated are approximately 75% of the Young's modulus values of the sample.

Spin coating of silicon wafer with polystyrene

Silicon wafers were first cleaned by sonication in ethanol and water, each for 15 minutes. Next, 3 mL of a 2% polystyrene solution in toluene was applied to fully cover the wafer surface. Spin coating was performed at 3000 rpm, with an acceleration of 500 rpm s^{-1}, for a duration of 1 minute (Laurell, WS-650MZ-23NPPB). The wafer was then dried in an oven at 50 °C for 1 hour.

Statistical analysis

A one-way ANOVA (α = 0.05) followed by Tukey's HSD multiple comparison test, as well as unpaired t-test, was conducted to assess statistical significance between groups. Results are presented as mean ± standard deviation (SD). All statistical analyses were performed using GraphPad Prism 9.

Author contributions

Conceptualization (Akbarinejad, Malmstrom, Fiedler); data curation (Malmstrom, Akbarinejad); formal analysis (Akbarinejad, Fiedler, Gito, Loho, Sherrell, Aw, Travas-Sejdic, Malmstrom); funding acquisition (Malmstrom); investigation (Akbarinejad, Fiedler, Gito, Loho, Sherrell, Aw, Malmstrom); methodology (Akbarinejad, Fiedler, Gito, Loho, Sherrell, Aw, Travas-Sejdic, Malmstrom); project administration (Akbarinejad, Malmstrom); supervision (Malmstrom); validation (Akbarinejad, Fiedler, Sherrell, Aw, Ellis, Travas-Sejdic, Malmstrom); visualization (Akbarinejad, Malmstrom); writing original draft (Akbarinejad, Fiedler); writing review & editing (Akbarinejad, Fiedler, Gito, Loho, Sherrell, Aw, Ellis, Travas-Sejdic, Malmstrom).

Conflicts of interest

There are no conflicts to declare.

Data availability

The authors declare that the data supporting the findings of this study are available within the paper and its supplementary information (SI). Supplementary information is available. See DOI: https://doi.org/10.1039/d6ta01041e.

Acknowledgements

The authors gratefully acknowledge the financial support provided by the Ministry of Business, Innovation and Employment (MBIE). We also express our appreciation for the ongoing support from the MacDiarmid Institute for Advanced Materials and Nanotechnology. The authors would like to thank Dr Eda Vella for assistance with AFM measurements, Catherine Hobbis for the help with SEM imaging and Dr Timothy Christopher for collecting the X-ray diffraction data. PCS acknowledges support

from RMIT University *via* the RMIT University Vice-Chancellors' Research Fellowship Scheme (2023).

References

1 N. Sezer and M. Koç, *Nano Energy*, 2021, **80**, 105567.
2 J. Chen, H. Liu, W. Wang, N. Nabulsi, W. Zhao, J. Y. Kim, M.-K. Kwon and J.-H. Ryou, *Adv. Funct. Mater.*, 2019, **29**, 1903162.
3 Y. Shan, E. Wang, X. Cui, Y. Xi, J. Ji, J. Yuan, L. Xu, Z. Liu and Z. Li, *Adv. Funct. Mater.*, 2024, **34**, 2400295.
4 D. Bai, S. Deng, Y. Li and H. Li, *Sens. Actuators, A*, 2023, **360**, 114515.
5 X. Gao, J. Yang, J. Wu, X. Xin, Z. Li, X. Yuan, X. Shen and S. Dong, *Adv. Mater. Technol.*, 2020, **5**, 1900716.
6 T. Morita, *Sens. Actuators, A*, 2003, **103**, 291–300.
7 C. Ghosal, S. K. Ghosh, K. Roy, B. Chattopadhyay and D. Mandal, *Nano Energy*, 2022, **93**, 106843.
8 S. Chen, J. Yang, S. Liu, Y. Huo, X. Cheng, L. Li and W. Ji, *Chem. Sci.*, 2026, **17**, 5416–5429.
9 B. Yang, Y. Zhang, S. Liu, Y. Huo and W. Ji, *Small*, 2026, e12690.
10 K. Chen, F. Wang, X. Sun, W. Ge, M. Zhang, L. Wang, H. Zheng, S. Zheng, H. Tang, Z. Zhou and G. Wu, *Bioact. Mater.*, 2025, **45**, 479–495.
11 J. Guo, C. Zhang, L. Li, M. Nie and Q. Wang, *Ind. Eng. Chem. Res.*, 2022, **61**, 14242–14250.
12 Y. Wu, Y. Ma, H. Zheng and S. Ramakrishna, *Mater. Des.*, 2021, **211**, 110164.
13 F. Mokhtari, Z. Cheng, R. Raad, J. Xi and J. Foroughi, *J. Mater. Chem. A*, 2020, **8**, 9496–9522.
14 R. Lay, G. S. Deijs and J. Malmström, *RSC Adv.*, 2021, **11**, 30657–30673.
15 M. Kim, Y. S. Wu, E. C. Kan and J. Fan, *Polymers*, 2018, **10**, 745.
16 L. Lu, W. Ding, J. Liu and B. Yang, *Nano Energy*, 2020, **78**, 105251.
17 R. Komljenovic, P. C. Sherrell, E. Goudeli, A. R. Rezk and L. Y. Yeo, *Mater. Horiz.*, 2025, **12**, 1207–1222.
18 Y. R. Wang, J. M. Zheng, G. Y. Ren, P. H. Zhang and C. Xu, *Smart Mater. Struct.*, 2011, **20**, 045009.
19 P. C. Sherrell, A. Šutka, M. Timusk and A. Šutka, *Small*, 2024, **20**, 2311570.
20 D. Kim, S. A. Han, J. H. Kim, J. H. Lee, S. W. Kim and S. W. Lee, *Adv. Mater.*, 2020, **32**, 1906989.
21 Z. Zhang, Z. Wang, X. Li, Y. Zheng and Z. Yang, *Chem. Rev.*, 2025, **125**, 9875–9929.
22 I. Chae, C. K. Jeong, Z. Ounaies and S. H. Kim, *ACS Appl. Bio Mater.*, 2018, **1**, 936–953.
23 F. Ram and K. Shanmuganathan, *Trends Carbohydr Res.*, 2021, **13**, 84.
24 E. Fukada, *J. Phys. Soc. Jpn.*, 1955, **10**, 149–154.
25 E. Fukada, *Wood Sci. Technol.*, 1968, **2**, 299–307.
26 E. Fukada, M. Date and N. Hirai, *J. Polym. Sci., Part C*, 1968, **23**, 509–517.
27 D. Denning, J. I. Kilpatrick, E. Fukada, N. Zhang, S. Habelitz, A. Fertala, M. D. Gilchrist, Y. Zhang, S. A. M. Tofail and B. J. Rodriguez, *ACS Biomater. Sci. Eng.*, 2017, **3**, 929–935.
28 Y. Shan, S. Liu, B. Wang, Y. Hong, C. Zhang, C. W. Lim, G. Zhang and Z. Yang, *Nat. Commun.*, 2021, **12**, 6066.
29 A. Šutka, P. C. Sherrell, N. A. Shepelin, L. Lapčinskis, K. Mālnieks and A. V. Ellis, *Adv. Mater.*, 2020, **32**, 2002979.
30 A. Akbarinejad, H. Fiedler, J. Nguyen, Z. Li, D. A. Gito, P. C. Sherrell, A. V. Ellis, K. Aw and J. Malmstrom, *Adv. Electron. Mater.*, 2024, **10**, 2400019.
31 R. T. Leon, P. C. Sherrell, A. Šutka and A. V. Ellis, *Nano Energy*, 2023, **110**, 108445.
32 A. Muxika, A. Etxabide, J. Uranga, P. Guerrero and K. de la Caba, *Int. J. Biol. Macromol.*, 2017, **105**, 1358–1368.
33 E. Praveen, S. Murugan and K. Jayakumar, *RSC Adv.*, 2017, **7**, 35490–35495.
34 G. de Marzo, V. M. Mastronardi, L. Algieri, F. Vergari, F. Pisano, L. Fachechi, S. Marras, L. Natta, B. Spagnolo and V. Brunetti, *Adv. Electron. Mater.*, 2022, 2200069.
35 S. Kim, D. Seol, X. Lu, M. Alexe and Y. Kim, *Sci. Rep.*, 2017, **7**, 41657.
36 O. Kwon, D. Seol, H. Qiao and Y. Kim, *Advanced Science*, 2020, **7**, 1901391.
37 E. Prokhorov, G. L. Bárcenas, B. L. España Sánchez, B. Franco, F. Padilla-Vaca, M. A. Hernández Landaverde, J. M. Yáñez Limón and R. A. López, *Colloids Surf., B*, 2020, **196**, 111296.
38 K. Ogawa, T. Yui and K. Okuyama, *Int. J. Biol. Macromol.*, 2004, **34**, 1–8.
39 J. Nicoletti, L. Puppulin, J. Routurier, S. Frroku, N. Loudhaief, C. Crestini, A. Perosa, M. Selva, M. Gigli, M. Back, P. Riello, D. De Fazio and G. A. Salvatore, *ACS Nano*, 2025, **19**, 35322–35332.
40 X. Han, Y. Xue, R. Lou, S. Ding and S. Wang, *Int. J. Biol. Macromol.*, 2023, **251**, 126191.
41 J. F. Mano, *Macromol. Biosci.*, 2008, **8**, 69–76.
42 C. Qiao, X. Ma, J. Zhang and J. Yao, *Carbohydr. Polym.*, 2019, **206**, 602–608.
43 J. Wang and S. Zhuang, *J. Clean. Prod.*, 2022, **355**, 131825.
44 J. F. Rubilar, R. M. S. Cruz, H. D. Silva, A. A. Vicente, I. Khmelinskii and M. C. Vieira, *J. Food Eng.*, 2013, **115**, 466–474.
45 A. Sionkowska, H. Kaczmarek, M. Wisniewski, J. Skopinska, S. Lazare and V. Tokarev, *Surf. Sci.*, 2006, **600**, 3775–3779.
46 D. Fengel, *Holzforschung*, 1993, **47**, 103–108.
47 G. Lawrie, I. Keen, B. Drew, A. Chandler-Temple, L. Rintoul, P. Fredericks and L. Grøndahl, *Biomacromolecules*, 2007, **8**, 2533–2541.
48 C. Qiao, X. Ma, X. Wang and L. Liu, *LWT–Food Sci. Technol.*, 2021, **135**, 109984.
49 M. Grossutti and J. R. Dutcher, *Biomacromolecules*, 2016, **17**, 1198–1204.
50 X. Wang, H. Bai, Z. Yao, A. Liu and G. Shi, *J. Mater. Chem.*, 2010, **20**, 9032–9036.
51 W. D. Callister Jr and D. G. Rethwisch, *Materials Science and Engineering: an Introduction*, John wiley & sons, 2020.

52 M. Vargas, A. Albors, A. Chiralt and C. González-Martínez, *Food Hydrocolloids*, 2009, **23**, 536–547.
53 F. Yang, J. Li, Y. Long, Z. Zhang, L. Wang, J. Sui, Y. Dong, Y. Wang, R. Taylor, D. Ni, W. Cai, P. Wang, T. Hacker and X. Wang, *Science*, 2021, **373**, 337–342.
54 S. K. Ghosh, P. Adhikary, S. Jana, A. Biswas, V. Sencadas, S. D. Gupta, B. Tudu and D. Mandal, *Nano Energy*, 2017, **36**, 166–175.
55 S. K. Karan, S. Maiti, S. Paria, A. Maitra, S. K. Si, J. K. Kim and B. B. Khatua, *Mater. Today Energy*, 2018, **9**, 114–125.
56 S. K. Ghosh and D. Mandal, *Appl. Phys. Lett.*, 2016, **109**, 103701.
57 S. Rajala, T. Siponkoski, E. Sarlin, M. Mettänen, M. Vuoriluoto, A. Pammo, J. Juuti, O. J. Rojas, S. Franssila and S. Tuukkanen, *ACS Appl. Mater. Interfaces*, 2016, **8**, 15607–15614.
58 S. Maiti, S. Kumar Karan, J. Lee, A. Kumar Mishra, B. Bhusan Khatua and J. Kon Kim, *Nano Energy*, 2017, **42**, 282–293.
59 N. R. Alluri, N. P. Maria Joseph Raj, G. Khandelwal, V. Vivekananthan and S.-J. Kim, *Nano Energy*, 2020, **73**, 104767.
60 G. de Marzo, V. M. Mastronardi, L. Algieri, F. Vergari, F. Pisano, L. Fachechi, S. Marras, L. Natta, B. Spagnolo, V. Brunetti, F. Rizzi, F. Pisanello and M. De Vittorio, *Adv. Electron. Mater.*, 2023, **9**, 2200069.
61 T. Jungk, Á. Hoffmann and E. Soergel, *Appl. Phys. Lett.*, 2007, **91**, 253511.
62 P.-K. Naito, Y. Ogawa, S. Kimura, T. Iwata and M. Wada, *J. Polym. Sci. B Polym. Phys.*, 2015, **53**, 1065–1069.
63 A. C. Jayasuriya, J. I. Scheinbeim, V. Lubkin, G. Bennett and P. Kramer, *J. Biomed. Mater. Res., Part A*, 2003, **66A**, 260–265.
64 H. Maeda and E. Fukada, *Biopolymers*, 1982, **21**, 2055–2068.
65 D. A. D. Gito, A. Akbarinejad, A. Dixon, T. Loho, M. Nieuwoudt, Q. Chen, L. J. Domigan and J. Malmström, *Biomacromolecules*, 2025, **26**, 514–527.
66 M. E. Dokukin and I. Sokolov, *Macromolecules*, 2012, **45**, 4277–4288.
67 ANSI/IEEE Std, 1988, pp. 176–1987, DOI: 10.1109/IEEESTD.1988.79638.
68 Y. Dobashi, D. Yao, Y. Petel, T. N. Nguyen, M. S. Sarwar, Y. Thabet, C. L. W. Ng, E. Scabeni Glitz, G. T. M. Nguyen, C. Plesse, F. Vidal, C. A. Michal and J. D. W. Madden, *Science*, 2022, **376**, 502–507.
69 S. M. Villa, V. M. Mazzola, T. Santaniello, E. Locatelli, M. Maturi, L. Migliorini, I. Monaco, C. Lenardi, M. Comes Franchini and P. Milani, *ACS Macro Lett.*, 2019, **8**, 414–420.
70 M. I. Hossain, H. Wang, L. Adhikari, G. A. Baker, A. Mezzetta, L. Guazzelli, P. Mussini, W. Xie and G. J. Blanchard, *J. Phys. Chem. B*, 2024, **128**, 1495–1505.
71 Ž. Simon, B. Dharmasiri, T. Harte, P. C. Sherrell and L. C. Henderson, *Mater. Horiz.*, 2024, **11**, 4321–4328.
72 W. C. Oliver and G. M. Pharr, *J. Mater. Res.*, 2004, **19**, 3–20.
73 J. C. Cheng and A. P. Pisano, *J. Microelectromech. Syst.*, 2008, **17**, 402–409.

